ISPRS Journal of Photogrammetry and Remote Sensing 119 (2016) 402–414

Contents lists available at ScienceDirect

ISPRS Journal of Photogrammetry and Remote Sensing

journal homepage: www.elsevier.com/locate/isprsjprs

Change detection of built-up land: A framework of combining pixel-based detection and object-based recognition

Pengfeng Xiao [a,b,c,d,*], Xueliang Zhang [a,b,c], Dongguang Wang [a,b,c], Min Yuan [a,b,c], Xuezhi Feng [a,b,c], Maggi Kelly [d]

[a] Department of Geographic Information Science, Nanjing University, Nanjing, Jiangsu 210023, China
[b] Collaborative Innovation Center of South China Sea Studies, Nanjing, Jiangsu 210023, China
[c] Jiangsu Center for Collaborative Innovation in Geographical Information Resource Development and Application, Nanjing, Jiangsu 210023, China
[d] Department of Environmental Sciences, Policy & Management, University of California, Berkeley, CA 94720, USA

ARTICLE INFO

Article history:
Received 10 January 2016
Received in revised form 7 May 2016
Accepted 4 July 2016

Keywords:
High-spatial resolution remote sensing image
Built-up land
Change detection
Pixel-based detection
Object-based recognition

ABSTRACT

This study proposed a new framework that combines pixel-level change detection and object-level recognition to detect changes of built-up land from high-spatial resolution remote sensing images. First, an adaptive differencing method was designed to detect changes at the pixel level based on both spectral and textural features. Next, the changed pixels were subjected to a set of morphological operations to improve the completeness and to generate changed objects, achieving the transition of change detection from the pixel level to the object level. The changed objects were further recognised through the difference of morphological building index in two phases to indicate changed objects on built-up land. The transformation from changed pixels to changed objects makes the proposed framework distinct with both the pixel-based and the object-based change detection methods. Compared with the pixel-based methods, the proposed framework can improve the change detection capability through the transformation and successive recognition of objects. Compared with the object-based method, the proposed framework avoids the issue of multitemporal segmentation and can generate changed objects directly from changed pixels. The experimental results show the effectiveness of the transformation from changed pixels to changed objects and the successive object-based recognition on improving the detection accuracy, which justify the application potential of the proposed change detection framework.

1. Introduction

China has experienced a rapid urban expansion over the past three decades because of its accelerated economic growth (Xiao et al., 2014). The urban expansion resulted in a continuous increase of land take, defined as the conversion of open spaces into artificial surfaces (i.e. built-up, road and rail networks) as well as green urban areas and sporting and leisure facilities (Artmann, 2014). Built-up is defined herein as the area occupied by buildings and its surrounding (Pesaresi et al., 2011). The change of built-up land has led to a series of issues including reductions in the efficient use of land, declining amounts of land for cultivation, environmental pollution, and ecological destruction. Thus, accurate determination of the changes on built-up land is important to facilitate proper urban planning proposals and to achieve sustainable development of both economy and environment.

Change detection is the process of identifying differences in the state of the same object or phenomenon on land through multiple observations carried out at different phases (Singh, 1989). The process uses multitemporal datasets to qualitatively analyse the temporal effects of objects or phenomena and quantify the changes (Hussain et al., 2013). Change detection studies with remote sensing data have been used in a wide variety of applications including land use and land cover, deforestation studies, natural disaster monitoring, as well as building damage assessments (Lu et al., 2004).

The technique of change detection has advanced with increases in the spatial resolution of remote sensing images and it has been used for applications at different spatial scales. Coarse-spatial resolution data such as Advanced Very High Resolution Radiometer (AVHRR) data and Moderate Resolution Imaging Spectroradiometer (MODIS) images are often practicable for large-scale change

* Corresponding author. Department of Geographic Information Science, Nanjing University, China.
E-mail address: xiaopf@nju.edu.cn (P. Xiao).

http://dx.doi.org/10.1016/j.isprsjprs.2016.07.003
0924-2716/

detection (Lu et al., 2004), e.g. global and national change mapping. Meanwhile, moderate-spatial resolution data such as Landsat and Système Probatoire Pour l'Observation de la Terre (SPOT) images are largely applied to change detection at the local and city scales (Nielsen et al., 2008).

Change detection based on coarse- and moderate-spatial resolution remote sensing images is processed primarily at the pixel level, which involves direct and post-classification comparisons (Coppin et al., 2004). Commonly used direct comparison methods include image differencing (Sohl, 1999), image ratioing (Prakash and Gupta, 1998), principal component analysis (Kwarteng and Chavez, 1998), and change vector analysis (Chen et al., 2003), etc. The challenge of using these methods is the determination of a suitable threshold for detecting change. They have relatively fast computation speeds and can delineate the geometric boundaries of changed regions. However, they cannot provide the "from-to" information of landscape classes. The post-classification comparison techniques (Yuan et al., 2005) involve the separate classification of data obtained at different phases before comparing the classified images. These methods provide complete change information on both geometric properties and attribute values, but the accuracy of detection is limited by the accuracy of the classification process.

The emergence of commercially available high-spatial resolution remote sensing images at the end of the 20th century has posed challenges to pixel-based change detection methods (Hussain et al., 2013). Common high-spatial resolution images include satellite images (e.g. IKONOS, QuickBird, WorldView, and Chinese newly launched GF-1), aerial photographs, and unmanned aerial vehicle (UAV) images, etc. Compared with coarse- and moderate-spatial resolution images, high-spatial resolution images contain detailed information of land objects for performing the detection of changes. Textural features are also more evident, which allows for the derivation of more change information for land objects through comparison analysis (Blaschke, 2010). As a result, change detection methods based on high-spatial resolution images have to be capable of processing large datasets efficiently and accurately, and this has become an active area of research (Jung, 2004; Carlotto, 2005; Gamba et al., 2006; Bovolo and Bruzzone, 2007; Bouziani et al., 2010; Du et al., 2012; Ban and Yousif, 2012; Volpi et al., 2013; Bruzzone and Bovolo, 2013; Yousif and Ban, 2013; Liu et al., 2015).

For change detection of high-spatial resolution images, other than the existing pixel-based methods stated above, the object-based image analysis (OBIA) has attracted extensive attention, that is, object-based change detection (OBCD) (Chen et al., 2012). The advantages of OBCD method for handling high-spatial resolution images include: (i) changed objects can be obtained directly without filtering and smoothing after change detection; (ii) the methods are not sensitive to geometric calibrations, so that pixel offsets between images acquired at different phases have little impact on the results; and (iii) objects in the images have spatial semantic connotations that increase the accuracy of change detection (Johansen et al., 2010).

One of the challenges of OBCD is the need for a proper segmentation method that effectively uses the multitemporal images to detect changes of both geometric properties and attribute values of land objects (Blaschke et al., 2014). Many researchers stacked all of the bands of the images obtained at two phases to segment changed and unchanged objects (Desclée et al., 2006; Im et al., 2008; Stow et al., 2008). In addition, Listner and Niemeyer (2011) proposed segmenting the first image to derive multiresolution segments, overlaying the boundaries on the other image, and then checking all segmentation mergers for consistency and removing those failed mergers. However, these two methods just detect the changes of the objects' attribute values, not the geometric properties. Thus, Chen et al. (2013) separately segmented two images acquired at different phases before analysing the corresponding object changes. Nevertheless, it is difficult to extract objects in a stable way in case no change in shape occurs between the two acquisition phases. Therefore, how to obtain the change information of objects' attribute values and geometric properties is one of the important issues that need to be resolved for OBCD.

Because of the limitations in both pixel- and object-based change detection, a framework of combining pixel-based detection and object-based recognition is proposed for change detection of built-up land from high-spatial resolution remote sensing images. An adaptive differencing method based on textural and spectral features is designed to obtain changed pixels, which are then formed as changed objects by a set of morphological operations. The changed objects are further filtered based on the morphological building index (MBI) to recognise changed objects on built-up land. As a consequence, the proposed framework takes advantage of the spectral and textural features and determines the changes of the geometric properties and attribute values of the built-up land. The transformation from changed pixels to changed objects makes the proposed framework distinct, which can help to overcome the limitations of pixel- and object-based change detection. The pixel-based change detection may result in fragmentation and incomplete expression of change because of the high-spatial resolution, while in the proposed framework the transformation to changed objects and the successive recognition of objects make the detected regions more complete and can improve the detection accuracy. The object-based change detection faces the challenge of multitemporal segmentation, to overcome which, the proposed framework generates changed objects from changed pixels directly, which can efficiently utilize multitemporal images and is easy to manipulate by avoiding the issue of multitemporal segmentation.

2. Method

The proposed change detection framework comprises three components as shown in Fig. 1: (i) detection of changed pixels, (ii) generation of changed objects, and (iii) recognition of changed objects on built-up land.

The first component aims to integrate spectral and textural features effectively for comprehensive detection of changed pixels and to avoid non-detection. This process will result in fragmentation and incomplete expression of change. Therefore, for the second component, hole and gap filling through morphological closing and opening operations are applied to eliminate false changed pixels, and this generates changed objects with complete shapes and concise boundaries. This step represents the transition from the pixel-based detection to object-based recognition. In the third component, changed objects are further filtered through the difference of MBI in two phases, thus leading to the identification of changed objects on built-up land. Generally in the framework, the first and third components can make use of other pixel-based change detection and object-based analysis methods to expand the application potential.

2.1. Detection of changed pixels

The target of the change detection was built-up land, for which textural features are more evident compared with other classes of land objects in high-spatial resolution images. Further, different types of buildings have distinctive characteristics in terms of the order of arrangement and density of the layout. Hence, it is necessary to select effective textural features for change detection based

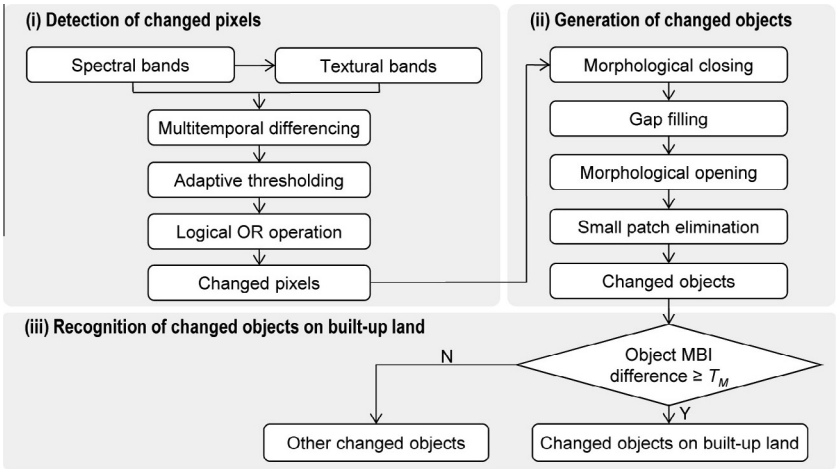

Fig. 1. Flowchart showing the three components and different steps used in the proposed change detection framework.

on the distinct characteristics of built-up land. In addition, the integration of spectral and textural features is also critical for change detection.

Specifically in the pixel-level change detection, we first calculated the spectral differences and textural differences separately. Then, we obtained the spectral changes and textural changes using an adaptive thresholding strategy on spectral differences and textural differences, respectively. Finally the two types of changes were combined using the logical OR operation. Thus the changed pixels contained both changes of spectra and texture. The details of each step of the pixel-level change detection are presented as follows.

2.1.1. Calculating textural features

The grey level co-occurrence matrix (GLCM) (Haralick et al., 1973) is a common method to describe image texture. It involves exploring the spatial correlation characteristics of grey levels as well as the spatial distribution relationship between pixels (Clausi, 2002). To select effective textural measures for built-up land change detection, we tested three types of subsets of high-spatial resolution images, which represented factory built-up land, residential built-up land, and cropland, respectively. The mean values of the nine measures of the GLCM, i.e. contrast, dissimilarity, homogeneity, angular second moment, energy, entropy, mean, variance, and correlation, were computed for the three types of images. The variance measure showed largest difference in the mean values between built-up land images and cropland image than the other measures. Thus, the GLCM variance measure was selected as the textural feature for change detection, which was used to describe differences in grey levels between adjacent pixels and represent the structural characteristics of objects on built-up land.

$$\text{GLCM variance} = \sum_{i=1}^{N}\sum_{j=1}^{N} P(i,j)(i-\mu)^2 \tag{1}$$

where $P(i, j)$ represents the probability of all possible pairs of adjacent pixel grey levels i and j for a selected distance d and direction angle θ, namely the GLCM. It is determined separately for θ equals to 0°, 45°, 90°, and 135°, as well as d equals to 1, 2, and 3 pixels. The values of 45° and 1 pixel were used in the study. μ represents the mean value of the GLCM. N represents the number of grey levels.

The GLCM variance measure was calculated from each spectral band of high-spatial resolution image. The window size for calculating texture feature was set as 7×7 pixels in this study and the effectiveness of window size on detection performance will be analysed in the experiment. The values of each textural band were then normalised as follows:

$$DN' = \frac{DN - DN_{\min}}{DN_{\max} - DN_{\min}} \times 255 \tag{2}$$

where DN and DN' are pixel values before and after normalisation, respectively; and $DN_{\max}$ and $DN_{\min}$ are the maximum and minimum pixel values before normalisation, respectively.

2.1.2. Generating differential images

For each spectral and textural band, the differential image was generated by calculating the differences between two phases as follows:

$$f(x,y) = |f^2(x,y) - f^1(x,y)| \tag{3}$$

where x and y are the row and column values of an pixel, respectively; $f^1(x, y)$ and $f^2(x, y)$ represent the pixel values at coordinate (x, y) at the former and later phases, respectively; and $f(x, y)$ is the pixel value of the band after differential processing.

2.1.3. Obtaining changed pixels

After obtaining the change magnitude of each band, we need to determine the thresholds between the changed and unchanged pixels. The response to change detection varied for each band. Specifically, differences existed between the contributions of textural and spectral features to change detection (Volpi et al., 2013). Consequently, it was not reasonable to apply a general threshold for segmentation of all the bands. Thus, an adaptive method was proposed to calculate the threshold, which was determined mainly by the mean and was adjusted by the standard deviation of each band.

$$f'(x,y) = \begin{cases} 1, & \text{if } f(x,y) \geqslant (\mu + T \cdot \sigma) \\ 0, & \text{otherwise} \end{cases} \tag{4}$$

where $f(x, y)$ and $f'(x, y)$ are the pixel values of a band before and after segmentation using the threshold, respectively; μ and σ are the mean and standard deviation of the band, respectively; T is the threshold parameter needed to be set, which includes T_S and T_T for spectral and textural bands, respectively. Pixels satisfying the distinguishing criterion were treated as changed pixels and assigned a value of 1. The others were treated as unchanged pixels, and assigned a value of 0.

Based on Eq. (4), the threshold values for each spectral or textural band could be adaptively adjusted according to the distribution

characteristics of the pixel values in that band by setting a T_S or T_T, respectively.

2.1.4. Logical OR operation

In order to take full advantage of the spectral and textural differences between various bands and to minimise the probability of non-detection, a logical OR operation was performed on the binary detection results from all the bands, as shown in Fig. 2. The spectral differences reflect the changes in the object interior while the textural differences produce the structural changes of objects. As long as the detection result of a particular band was 1, it would ultimately be treated as a changed pixel. Then after the logical OR operation, the detected changed pixels include both the interior and structural changes of objects.

2.2. Generation of changed objects

The results from the detection of changed pixels were fragmented, as shown in the example of Figs. 2 and 3. This could be due to (i) changes over time in the details of land objects, (ii) high internal heterogeneity within regions leading to large numbers of holes and gaps, and (iii) small patches of no significance in the detection results, which were produced by registration errors, sensor angles, and image noise.

In order to facilitate subsequent object analysis, we designed four steps of post-processing operations to generate changed objects with accurate borders and complete shapes from the changed pixels as illustrated in Fig. 3: (i) morphological closing operation, (ii) gap filling, (iii) morphological opening operation, and (iv) elimination of small patches.

A morphological closing operation is the process of applying dilation to the image, followed by erosion using a structuring element. The aim is to fill holes within patches to form closed and interconnected regions. The key parameter of the closing operation is the structuring element. If the dimensions of the structuring element are set too large, there will be over-merger of adjacent regions and a large false changed region will form. In the reverse situation, the effect of hole filling will not be sufficiently apparent. Thus, the structuring element is dependent on the pattern of changed pixels and needs to be set cautiously. We set it as a square structuring element with 3×3 pixels by the trial-and-error strategy. After the closing operation, over-fragmentation of the detection results was effectively improved as shown in Fig. 3d.

Next, the gaps within the changed regions were filled, i.e. were relabelled as changed pixels, which made the changed information more complete, as shown in Fig. 3e.

The morphological opening operation was applied afterwards in which erosion was conducted on the image, followed by dilation operation. The aim of the opening operation is to break those narrow connections between regions that are smaller than the structuring element. Moreover, it can eliminate single pixel noise and result in regions with regular shapes. Multiple tests have confirmed that desirable results are obtained when the dimensions of the structuring element used for the opening operation are slightly larger than those used for the closing operation. Hence, a square structuring element with 5×5 pixels was used for the opening operation. The results in Fig. 3f show the effectiveness of this step.

Small insignificant patches still existed after the opening processing. Hence, an area threshold (T_A) can be used to remove these. For this study, T_A was set as 200 m^2 following the *National Specification of Land and Mine Monitoring Based on Remote Sensing Images* issued by the Ministry of Land and Resources of China in 2010. Accordingly, the detection results became clearer with complete detection of most of the large changed regions as shown in Fig. 3g. The results were also closer in shape to the changed regions that were interpreted by remote sensing experts as reference image shown in Fig. 3h.

Finally, a region formed by the interconnected changed pixels was labelled as a single object. The generation of changed objects was completed after labelling all the regions.

2.3. Recognition of changed objects on built-up land

The categories of generated changed objects include: (i) newly built-up land, (ii) changes from built-up to non-built-up land,

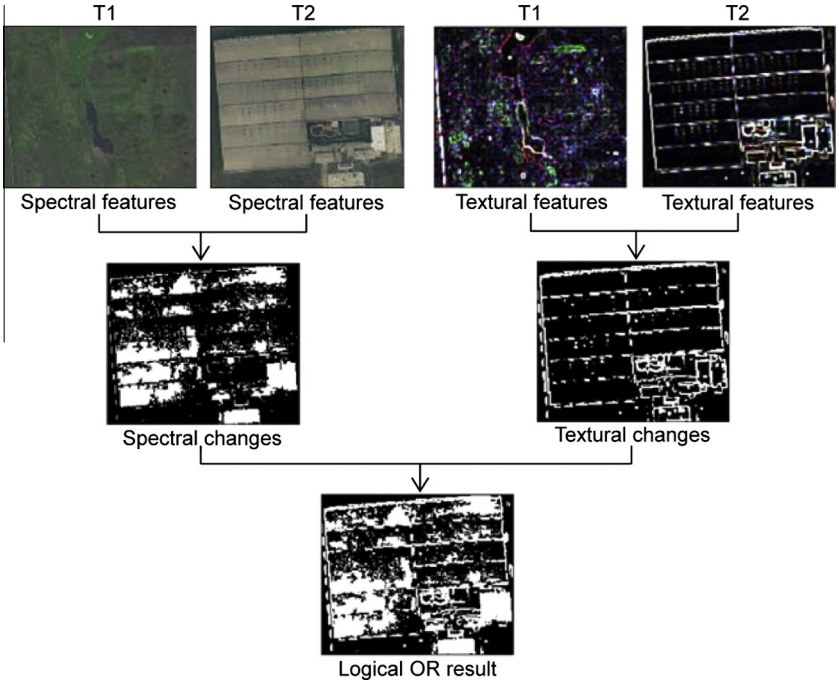

Fig. 2. An example showing the effectiveness of logical OR operation on combining spectral changes and textural changes.

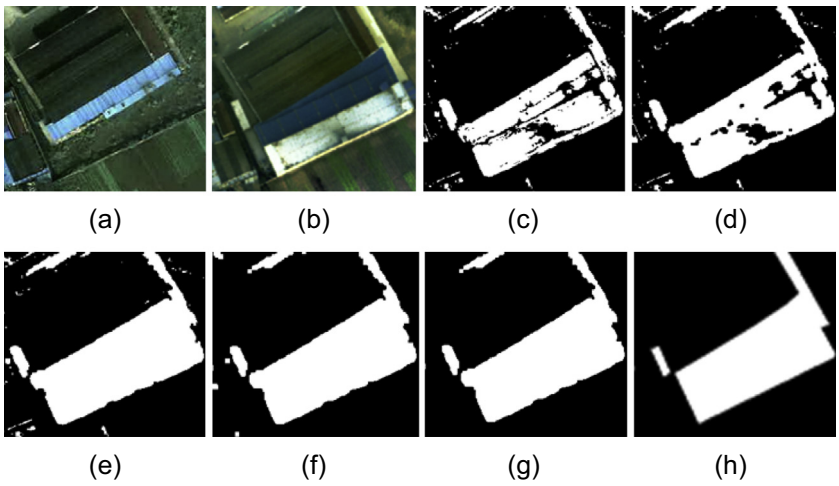

Fig. 3. An example showing the post-processing of changed pixels for generating changed objects. (a) Image before change; (b) image after change; (c) detected changed pixels; (d) result after the morphological closing operation; (e) result after gap filling; (f) result after the morphological opening operation; (g) result after elimination of small patches; (h) manually interpreted changed objects as reference.

(iii) changes within built-up land, and (iv) changes within non-built-up land. The first two categories are the main targets for change detection of built-up land. Specifically, newly built-up land is the most important category for monitoring land resources in China. Therefore, an object-level recognition method was further designed to identify those changed objects on built-up land.

The MBI proposed by Huang et al. (2014) was adopted in the study to recognise changed objects on built-up land. The basic idea of MBI is to build a relationship between the spectral-spatial characteristics of buildings and the morphological operators. It first calculates the maximal digital number of the multispectral bands for each pixel, and then the differential morphological profiles of the top-hat transformation (TH-DMP) with multiscale and multidirectional structural elements are calculated, and finally the MBI is defined as the average of the multiscale and multidirectional TH-DMP. Generally, MBI can highlight buildings and suppress background, which makes it has the potential to indicate building changes from high-spatial resolution images. Theoretically, the changes between built-up land and non-built-up land in two phases will present large MBI differences, while the changes within built-up land or non-built-up land will have small MBI differences.

For each changed object O_i, we calculated the mean MBI value at the former phase (MBI_i^1) and the later phase (MBI_i^2), respectively. Then the MBI difference $D(MBI_i)$ was calculated according to Eq. (5). Finally, a thresholding strategy was applied as shown in Eq. (6). The changed type C_i was determined as changed object on built-up land if its MBI difference larger than the threshold parameter T_M, otherwise, it was recognised as other changed object.

$$D(MBI_i) = |MBI_i^2 - MBI_i^1| \tag{5}$$

$$C_i = \begin{cases} 1, & \text{if } D(MBI_i) \geqslant T_M \\ 0, & \text{otherwise} \end{cases} \tag{6}$$

2.4. Accuracy assessment

The "ground-truth" objects on changed built-up land were delineated using an expert interpretation method with a field investigation. This yielded the reference image. The accuracy rate (*AR*), false detection rate (*FDR*), and overall accuracy (*OA*) were calculated to assess the accuracy of the detection results.

$$AR = \frac{S_r}{S_c} \tag{7}$$

$$FDR = \frac{S_a - S_r}{S_a} \tag{8}$$

$$OA = \frac{S_r + S_n}{S} \tag{9}$$

where S_r is the number of changed pixels that were correctly detected in the result image, S_c is the number of changed pixels in the reference image, S_a is the number of changed pixels in the result image, S_n is the number of non-changed pixels that were correctly detected in the result image, and S is the overall number of pixels in the image. The *AR* measure reflects the missed alarms of the change detection result and the *FDR* measure reflects the false alarms. They should be combined to indicate the detection capability, i.e., the large *AR* value and small *FDR* value indicate the better change detection accuracy. In addition, the *OA* measure reflects the overall change detection accuracy by considering both the changed and unchanged pixels.

3. Experimental results

The proposed framework were implemented using the C# language. Six datasets including one IKONOS dataset, two GF-1 datasets, and three aerial datasets were used to show the detection results. The pixel-level change detection results, changed objects after post-processing, and the final changed objects on built-up land after recognition will be presented. Specifically, the effectiveness of selected textural feature, designed post-processing, and adopted MBI feature will be analysed. Furthermore, the proposed change detection framework was compared with pixel-based change vector analysis method (Johnson and Kasischke, 1998; Bovolo et al., 2012) and the state-of-the-art object-based change detection method (Bovolo, 2009). Totally there are three threshold parameters T_S, T_T, and T_M needed to be set in the proposed method. In this study, we did not pay attention to automatically setting optimal threshold parameters. Thus, we used the trial-and-error strategy to set these parameters.

3.1. Datasets

Six datasets including a pair of IKONOS images, two pairs of GF-1 images, and three pairs of aerial photographs were investigated. The datasets are shown in Fig. 4 and their details are listed in Table 1. All the datasets are located in Jiangsu Province of eastern

China, in which the cities have undergone rapid economic transition and upgrades, which have led to significant changes of the land uses with rapid increases in the amount of land used for industrial and residential purposes. Dataset 1 (DS1) is composed of multitemporal IKONOS images of an suburb area of Nanjing City. Dataset 2 (DS2) is a pair of GF-1 images of an industrial area of Nanjing City. Dataset 3 (DS3) contains two GF-1 images in the suburb area of Xuzhou City. The spatial resolution of multispectral bands of DS1–DS3 was improved by applying the Gram-Schmidt pan-sharpening method implemented in the ENVI software. The other three datasets (DS4–DS6) consist of multitemporal aerial photographs on three suburb areas of Changzhou City. The main changes in these datasets are newly-built buildings along with a few rebuilt ones. The main challenge of change detection lies in the fake changes of built-up land, e.g., the spectral changes of roads and buildings, and the emergence of bare soil, which may result in false alarms because of the significant spectral changes.

The datasets were preprocessed as two steps: (i) geometric registration by a polynomial function based on 25 ground control points (GCPs) where the overall root mean square (RMS) error is less than 0.5 pixels; and (ii) radiometric correction using pseudo invariant features (Schott et al., 1988).

In order to evaluate the proposed change detection framework, the changed objects on built-up land in these six datasets were visually analysed and manually delineated by a specialist, and were reviewed by a second specialist to catch errors. Both the interpreter and reviewer were independent of this study. The reference maps are also shown in Fig. 4.

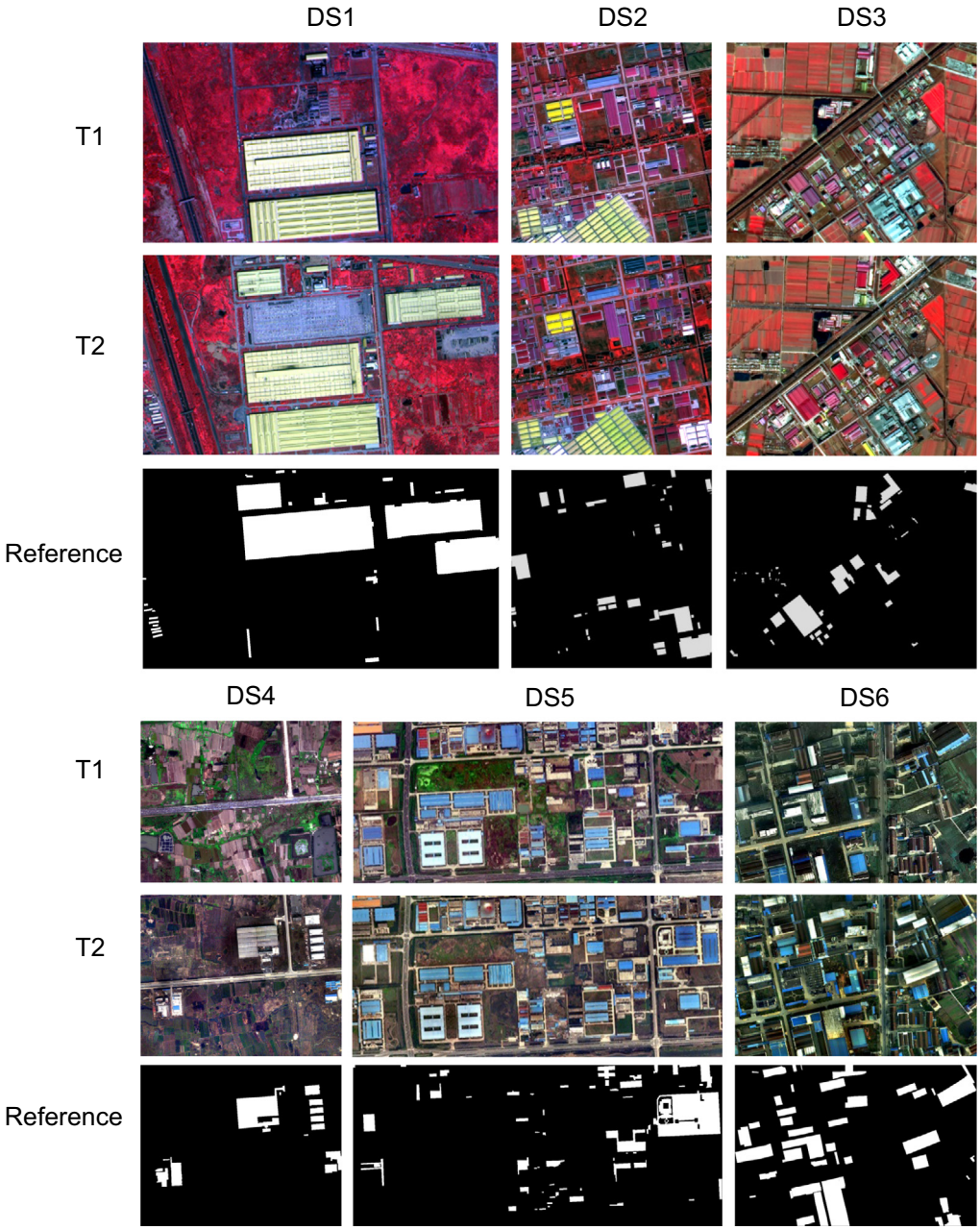

Fig. 4. Six datasets and reference maps. The satellite images DS1–DS3 are shown with band combination of near infrared, red, and green bands. The aerial photographs DS4–DS6 are shown with true colour. (For interpretation of the references to colour in this figure legend, the reader is referred to the web version of this article.)

Table 1
Details of six datasets.

Dataset	Platform	Size (pixels)	Spatial resolution	Available bands	Year (T1)	Year (T2)	Location
DS1	IKONOS	900 × 1600	1 m	NIR, R, G, B	2000	2009	Nanjing, Jiangsu, China
DS2	GF-1	950 × 950	2 m	NIR, R, G, B	2013	2015	Nanjing, Jiangsu, China
DS3	GF-1	800 × 1000	2 m	NIR, R, G, B	2013	2016	Xuzhou, Jiangsu, China
DS4	Aerial	800 × 1000	1 m	R, G, B	2008	2012	Changzhou, Jiangsu, China
DS5	Aerial	700 × 1600	1 m	R, G, B	2008	2012	Changzhou, Jiangsu, China
DS6	Aerial	800 × 1200	0.5 m	R, G, B	2008	2012	Changzhou, Jiangsu, China

3.2. Detected changed pixels

In this part, the effectiveness of spectral and textural features on pixel-level change detection is analysed. Firstly, the influence of window size (*WS*) for textural feature is presented in Table 2. In order to determine the optimal window size for computing textural feature, we tested five sizes, namely 3 × 3, 5 × 5, 7 × 7, 9 × 9, and 11 × 11 pixels, for all the six datasets. We set the same values for the parameters T_S and T_T for each dataset. Table 2 shows that the accuracies of detected changed pixels are not significantly different with each other when setting different window sizes. Compared with other window sizes, the window size 7 × 7 pixels can achieve slightly higher *AR* and *OA* and lower *FDR* for DS1–DS4, and show slightly lower accuracy than larger and smaller windows for DS5 and DS6, respectively. From visual analysis, the outlines of buildings were distinct when using a small window, namely 3 × 3 pixels, but the details inside building borders were detected excessively, which will result in false detections of built-up land change. The excessive details were reduced when using a window with 5 × 5 or 7 × 7 pixels, but further reductions were not possible because the outlines of buildings became blurred when using windows with 9 × 9 pixels or larger. Thus, the window size of 7 × 7 pixels was used in the study.

The accuracies of detected changed pixels by setting different T_S and T_T for all the datasets are presented in Fig. 5. Comparing the curves using only spectral features with those using both spectral and textural features, we can see that the textural feature can improve the detection accuracy while at the same time increase the false alarms. The improvement is getting larger when the parameter T_T is setting smaller, which is because the logical OR operation results in more changed pixels. When T_S is setting larger, both the detection accuracy and false alarms are decreased because fewer changed pixels are detected.

In order to clearly present the differences caused by the textural feature, the pixel-level change detection accuracies are shown in Table 3, from which we can see that the textural feature has the potential to improve the change detection capability by improving *AR* and *OA*, and at the same time lowering *FDR*.

3.3. Effectiveness of post-processing

In the pixel-level change detection result shown in the first and third rows of Fig. 7, the changed pixels are distributed all over the image due to the effects of local details and image noise. In addition, the changed regions are fragmented because of the heterogeneity of objects in high-spatial resolution images. The

Table 2
Pixel-level detection accuracy by using GLCM textural features with different window sizes.

WS	DS1 (T_S = 1.2, T_T = 3.5)			DS2 (T_S = 1.2, T_T = 2.0)			DS3 (T_S = 1.0, T_T = 3.0)			DS4 (T_S = 1.4, T_T = 3.0)			DS5 (T_S = 1.5, T_T = 3.4)			DS6 (T_S = 1.0, T_T = 1.9)		
	AR	*FDR*	*OA*	*AR*	*FDR*	*OA*	*AR*	*FDR*	*OA*	*AR*	*FDR*	*OA*	*AR*	*FDR*	*OA*	*AR*	*FDR*	*OA*
3 × 3	0.717	0.461	0.844	0.789	0.697	0.858	0.785	0.792	0.826	0.836	0.577	0.907	0.700	0.610	0.886	0.751	**0.488**	**0.837**
5 × 5	0.715	0.465	0.843	0.802	0.681	0.866	0.789	0.791	**0.827**	0.841	0.570	0.909	0.703	0.605	0.887	0.752	0.490	0.836
7 × 7	**0.721**	**0.448**	**0.850**	0.811	**0.677**	**0.868**	0.792	**0.790**	**0.827**	**0.842**	**0.568**	**0.910**	0.702	0.597	0.890	**0.754**	0.491	0.836
9 × 9	0.710	0.479	0.836	0.811	0.679	0.867	0.793	0.791	0.826	0.840	0.569	0.909	0.704	0.594	0.891	**0.754**	0.493	0.835
11 × 11	0.710	0.480	0.836	**0.819**	0.681	0.865	**0.794**	0.791	0.826	0.839	0.571	0.909	**0.706**	**0.592**	**0.892**	**0.754**	0.494	0.835

The bold values indicate the highest accuracies in each condition.

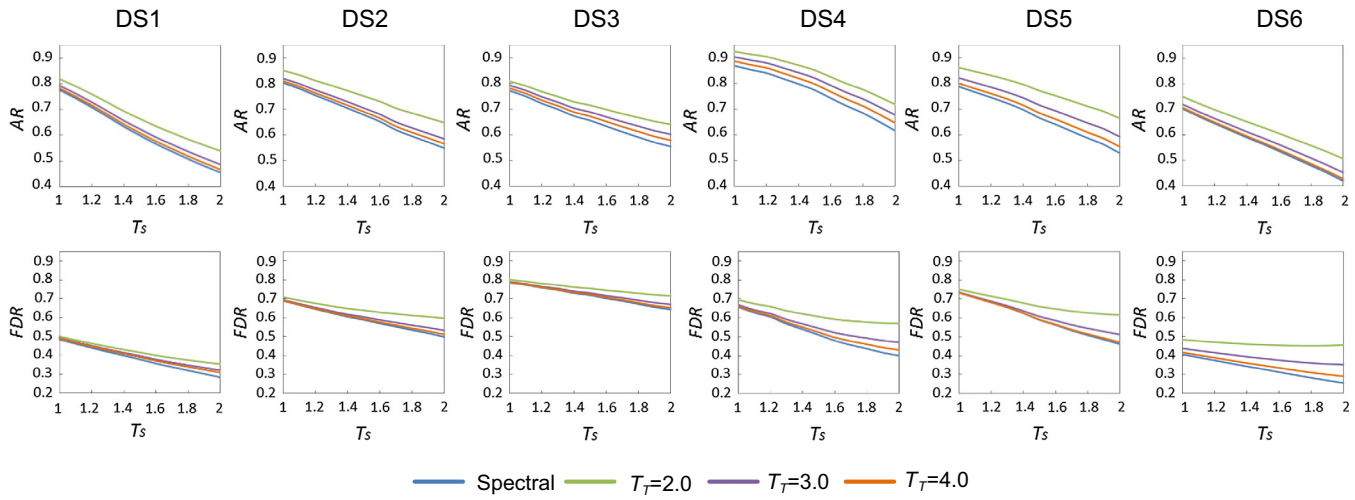

Fig. 5. Accuracies of pixel-level change detection results by setting different T_S and T_T. The spectral curves represent change detection with spectral bands only.

Table 3
Comparisons of pixel-level change detection accuracies with or without using textural features.

Features	DS1			DS2			DS3			DS4			DS5			DS6		
	AR	*FDR*	*OA*	*AR*	*FDR*	*OA*	*AR*	*FDR*	*OA*	*AR*	*FDR*	*OA*	*AR*	*FDR*	*OA*	*AR*	*FDR*	*OA*
Spectral	0.834	0.536	0.804	0.802	0.690	0.861	0.814	0.817	0.792	0.819	0.568	0.910	0.827	0.779	0.747	0.829	0.513	0.824
$T_T = 2.0$	0.844	**0.524**	**0.812**	0.811	**0.677**	**0.869**	**0.827**	0.815	0.793	**0.825**	0.592	0.902	**0.831**	**0.715**	**0.815**	0.823	0.517	0.822
$T_T = 3.0$	**0.847**	0.541	0.800	**0.819**	0.695	0.857	0.813	**0.806**	**0.806**	0.821	**0.545**	**0.917**	0.822	0.736	0.798	0.821	**0.505**	**0.829**
$T_T = 4.0$	0.839	0.539	0.802	0.809	0.691	0.860	0.822	0.818	0.790	0.820	0.551	0.916	0.821	0.759	0.773	**0.832**	0.518	0.821

The bold values indicate the highest accuracies in each condition.

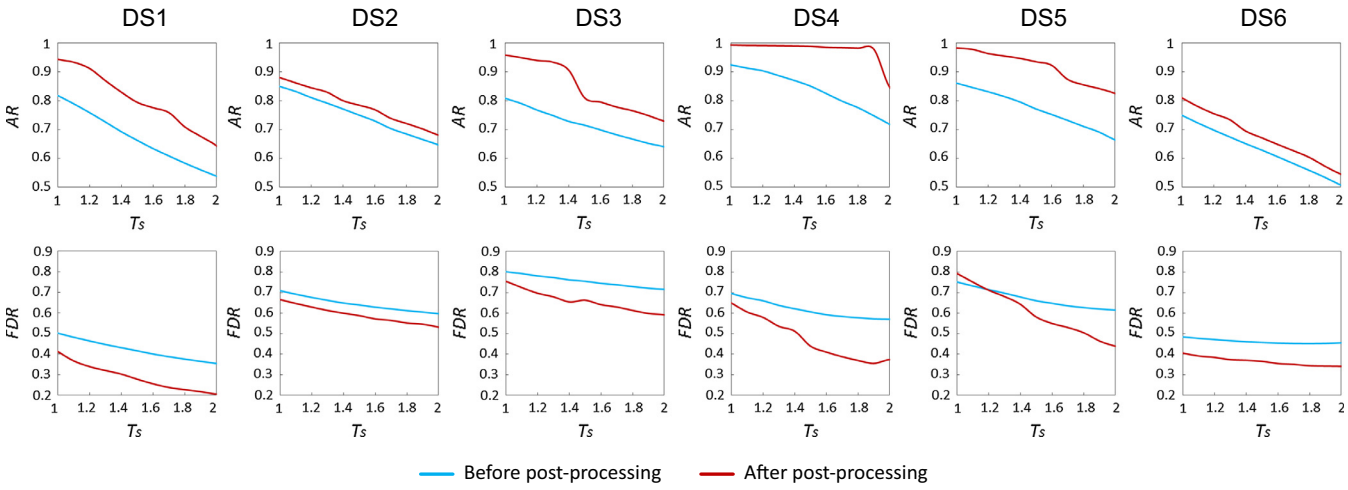

Fig. 6. Accuracies of change detection results before and after post-processing. The parameter T_T is set as 2.0.

post-processing operations are designed to remove the meaningless changed pixels and improve the completeness of changed regions. Hence, the effectiveness of post-processing operations on improving the detection accuracy and completeness of changed regions is analysed in this part.

The accuracies of changed pixels before post-processing and changed objects after post-processing for the six datasets are presented in Fig. 6, where the detection features and thresholding parameters are set the same for each dataset to clearly show the accuracy difference caused by the proposed post-processing operations. The textural thresholding parameter T_T is set as 2.0 because we are not optimizing the parameters in this part but just showing the effectiveness the post-processing operations. Fig. 6 shows that the post-processing operations can significantly improve the detection accuracy and at the same time decrease the false alarms for all the datasets. For DS1, DS3–DS5, both the increment of *AR* and the decrease of *FDR* are larger than 10%. The detection capability improvement for DS2 and DS6 is less significant, but the *AR* increment and *FDR* decrease are still over 5%. This demonstrates the effectiveness of post-processing on improve change detection capability.

In order to further explain the effectiveness of post-processing, the changed pixels and changed objects are presented in Fig. 7, together with accuracy values of each detection result. Similar to that of Fig. 6, we set the T_S and T_T parameters as 1.4 and 2.0 for all the datasets because we just aim at showing the difference caused by the post-processing operations. Compared with the pixel-level change detection result, the completeness of the changed regions is significantly improved after post-processing. Especially, the large changed regions are effectively gap-filled. The improvement of completeness is mainly due to the morphological closing and gap filling operations, which decreases the miss alarms and leads to an increase in the detection accuracy. Separately, the meaningless changed pixels are removed after post-processing, which make the results of changed objects very "clean". This is due to the procedures of morphological opening operation and elimination of small patches, which can effectively remove false changed regions that are caused by image noise, local details, and registration errors, thereby reducing the false alarms.

3.4. Comparison with existing change detection methods

In this part, the change detection results of the proposed method are compared with those produced by both pixel- and object-based methods. The pixel-based change vector analysis (CVA) method (Johnson and Kasischke, 1998) and compressed CVA (C^2VA) method (Bovolo et al., 2012) were selected for comparison to show the effectiveness of separately adaptive thresholding of spectral and textural features and the logical OR operation. The compared object-based change detection methods adopted multiresolution segmentation technique (Baatz and Schäpe, 2000) and object-based change vector analysis (OBCVA) (Bovolo, 2009), which was to show the effectiveness of post-processing operations on utilising multitemporal changed pixels to generate changed objects. The multitemporal image segmentation were performed in two different ways: (i) stacking all of the bands of the former and later phases to segment the combined image (combined OBCVA); and (ii) separately segmenting the images of the former and later phases and then using the raster overlay function to connect and compare objects (separated OBCVA) (Chen et al., 2013).

The same spectral and textural features were used and the same post-processing procedures were applied in the compared methods. In both the compared pixel- and object-based methods, there was a thresholding parameter of change magnitude to be set, which was named as T_1, T_2, T_3, and T_4, for the pixel-based CVA, C^2VA, combined OBCVA, and separated OBCVA, respectively. We set a series of values for these thresholding parameters similar to those in Figs. 5 and 6, and selected detection results that have either similar detection accuracy or similar false alarms for

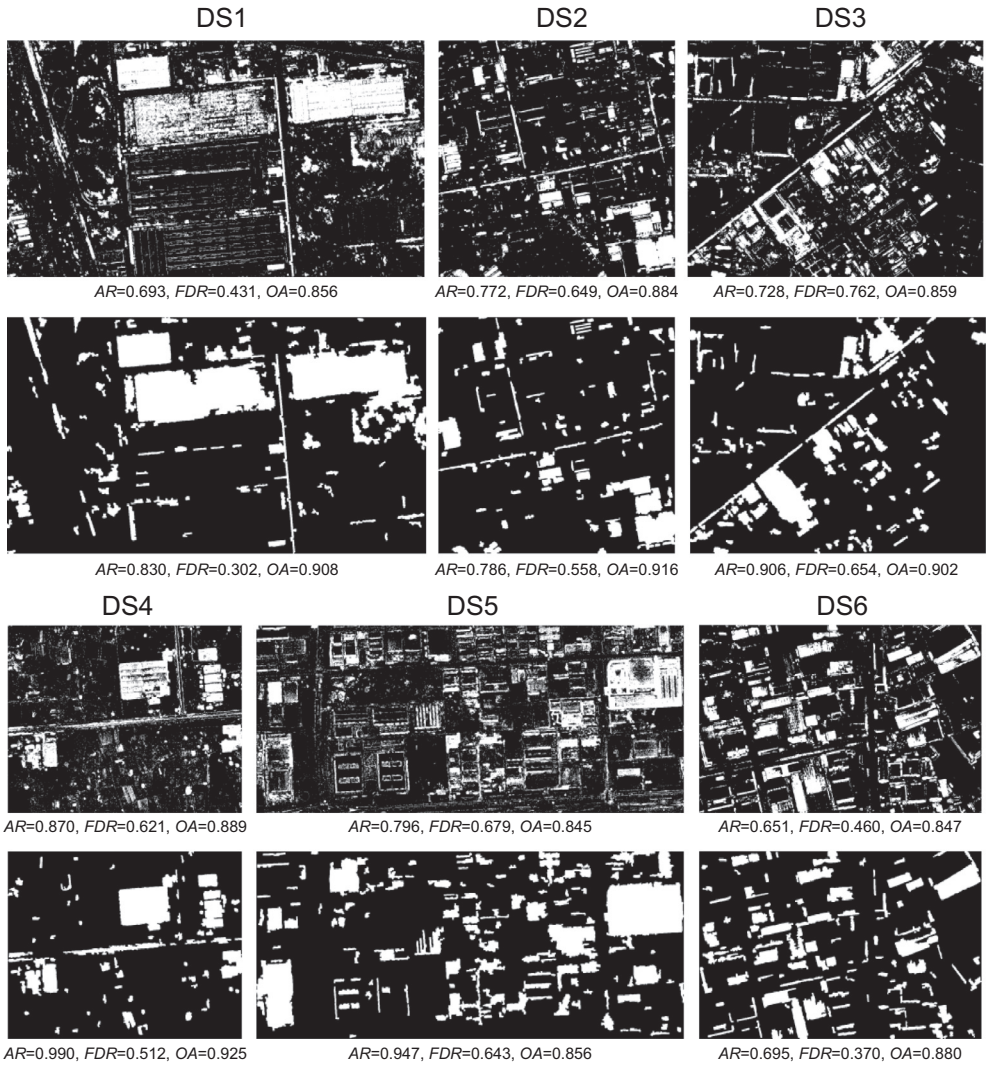

Fig. 7. Change detection results before (the first and third rows) and after (the second and forth rows) post-processing. The parameters T_S and T_T for each dataset are set as 1.4 and 2.0, respectively.

comparison. For C^{2}VA, the parameter of change direction was set by analysing the scatterogram to remove changes on non-built-up land. For OBCVA, we needed to set the segmentation parameters, including the scale parameter and shape parameter for the adopted multiresolution segmentation method. The parameter values were determined using the trial-and-error strategy, and the segmentation results that can result in the highest change detection accuracy were selected for comparison. Specifically, the scale parameter and shape parameter were set as (50, 0.4), (30, 0.5), (30, 0.5), (30, 0.3), (30, 0.4), and (30, 0.5) for DS1–DS6, respectively.

The change detection results and the corresponding detection accuracies are presented in Fig. 8 and Table 4, respectively. The main differences among the results of the six methods are marked with orange in Fig. 8. For DS2–DS6, the proposed method can achieve lower false alarms and thus higher overall accuracy. For DS1, the proposed method performs poorlier than the CVA and C^{2}VA methods, and achieves comparable accuracy to the OBCVA methods, which is mainly caused by the falsely detected roads. However, in most cases, the proposed method can achieve apparently better detection capacity than the pixel-based CVA method, which reflects the effectiveness of the designed pixel-based detection method and the logical OR operation. The C^{2}VA has lower false alarms than that of the CVA because that the feature of change direction can remove the changes of non-built-up land, so that the C^{2}VA achieves closer accuracy to the proposed method than that of the CVA. The proposed method can achieve better detection capacity than the two OBCVA methods in most cases, which verifies that the designed post-processing operations result in the effective utilization of multitemporal information by transforming the changed pixels to changed objects.

3.5. Recognised changed objects on built-up land

Since only the spectral and textural features were used in the pixel-level change detection component, the generated changed objects after post-processing cannot assure to be on built-up land. Hence, the MBI feature was adopted in the object-based recognition component to identify changed objects on built-up land. The effectiveness of the MBI feature on indicating changed built-up objects are shown in this part.

Based on the changed objects produced by the proposed change detection method in Fig. 8, the object-based recognition was applied using the MBI feature and the results and corresponding accuracies are shown in Fig. 9 and Table 5. As the recognition step focuses on removing several types of unwanted changed objects, it cannot improve the detection accuracy but aims to decrease the

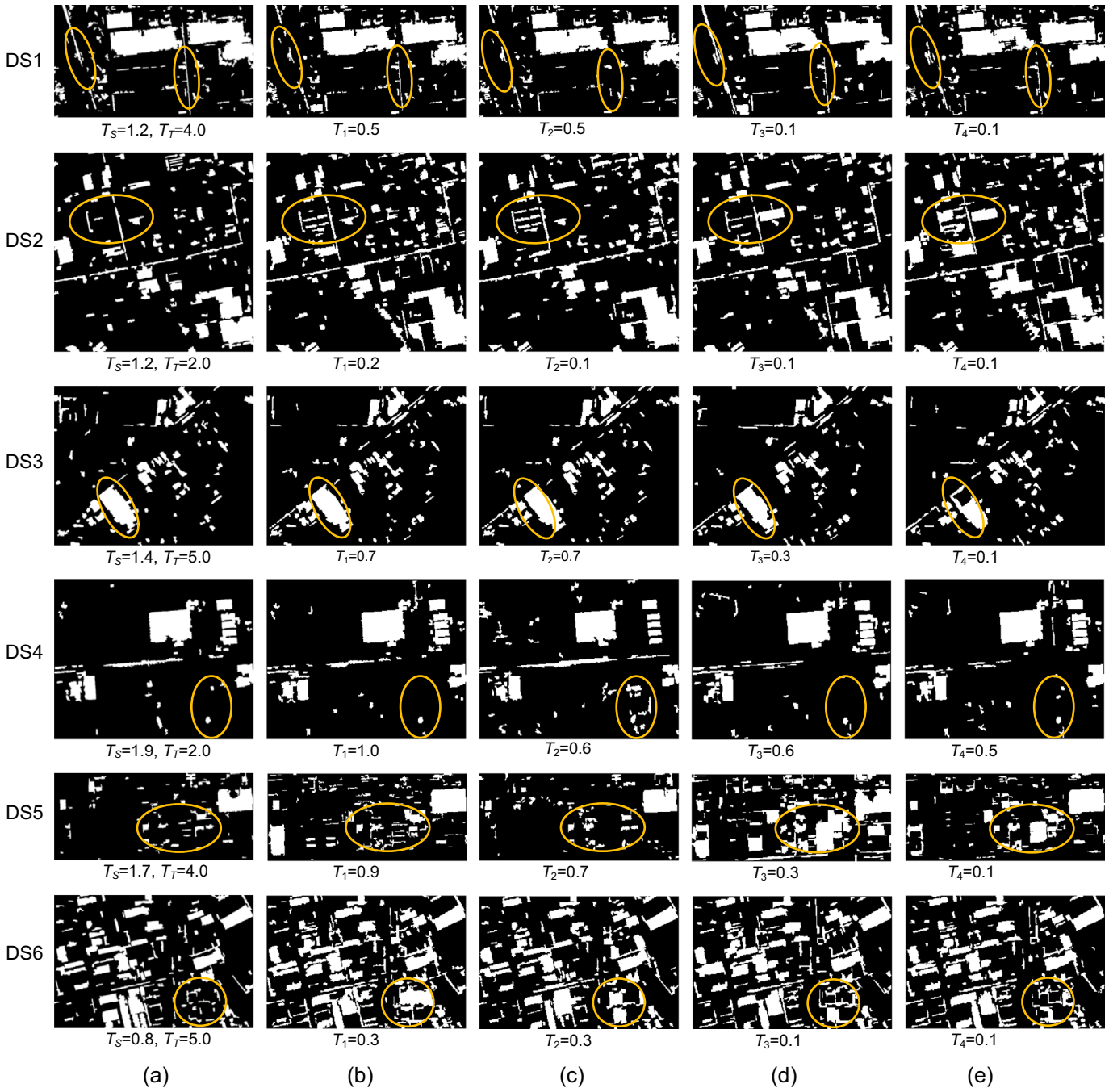

Fig. 8. Change detection results of (a) proposed method; (b) pixel-based CVA; (c) pixel-based C^2VA; (d) combined OBCVA; (e) separated OBCVA. The parameters T_1, T_2, T_3, and T_4 represent thresholds for pixel-based CVA, pixel-based C^2VA, combined OBCVA, and separated OBCVA, respectively. The marked regions with orange indicate the main differences among results of different methods.

Table 4
Accuracies of the results of the proposed change detection method and the compared pixel- and object-based change detection methods.

Method	DS1			DS2			DS3			DS4			DS5			DS6		
	AR	*FDR*	*OA*	*AR*	*FDR*	*OA*	*AR*	*FDR*	*OA*	*AR*	*FDR*	*OA*	*AR*	*FDR*	*OA*	*AR*	*FDR*	*OA*
Proposed	0.900	0.313	0.912	0.835	**0.594**	**0.903**	0.866	**0.553**	**0.935**	0.979	**0.355**	**0.960**	**0.806**	**0.307**	**0.955**	**0.822**	**0.361**	**0.892**
Pixel-based CVA	**0.902**	0.257	0.929	0.825	0.679	0.866	**0.869**	0.563	0.932	0.979	0.364	0.959	0.797	0.584	0.892	0.812	0.515	0.823
Pixel-based C^2VA	0.898	**0.233**	**0.935**	**0.836**	0.639	0.885	0.868	0.559	0.933	0.954	0.402	0.951	0.824	0.318	0.954	0.812	0.444	0.859
Combined OBCVA	0.900	0.295	0.917	0.833	0.655	0.878	0.834	0.564	0.932	0.963	0.393	0.953	0.759	0.763	0.780	0.810	0.469	0.847
Separated OBCVA	0.885	0.283	0.919	0.790	0.718	0.845	0.703	0.604	0.926	**0.983**	0.383	0.955	0.793	0.599	0.886	0.805	0.451	0.856

The bold values indicate the highest accuracies in each condition.

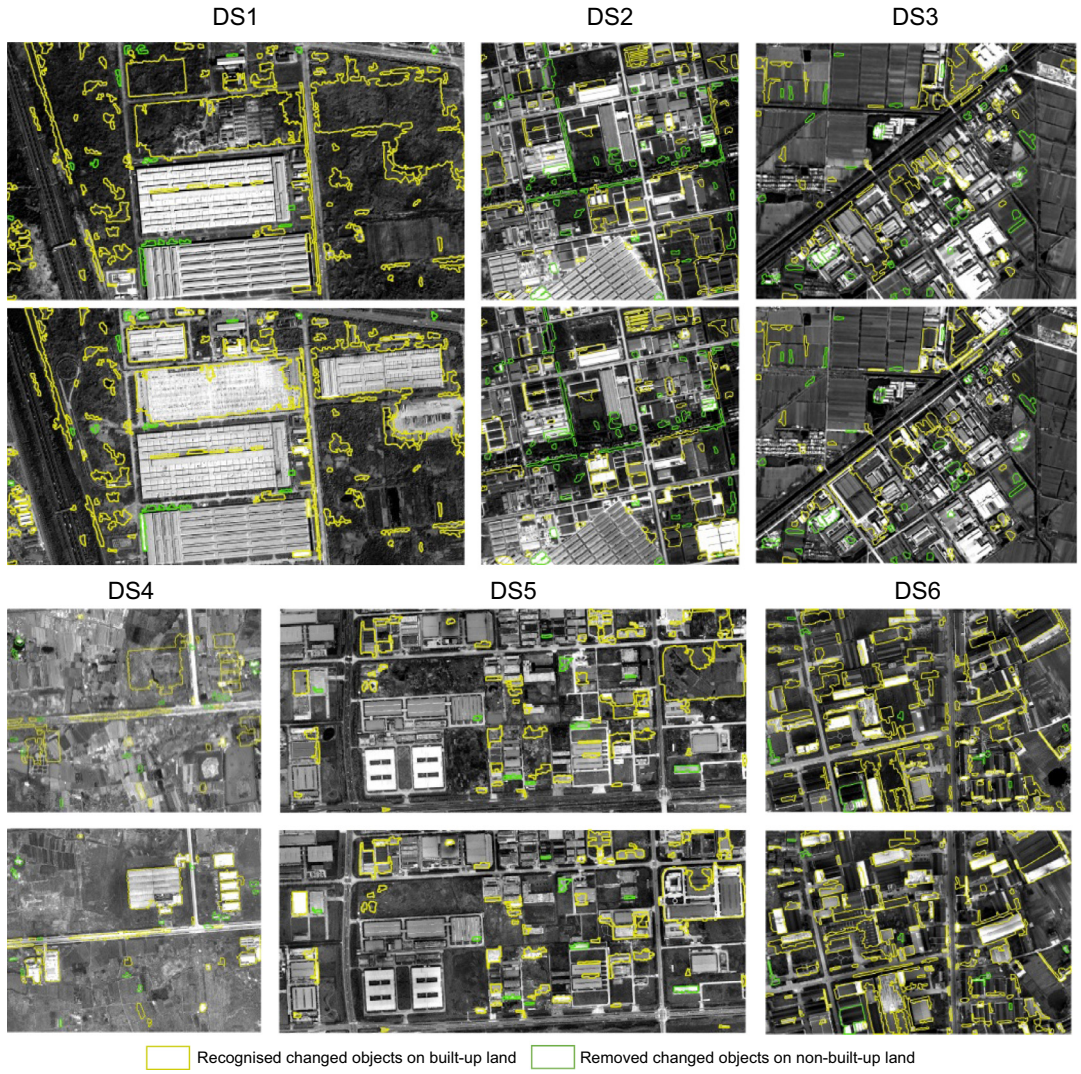

Fig. 9. Recognised changed objects on built-up land and removed changed objects on non-built-up land in the recognition step. The changed objects before recognition are shown in Fig. 8.

Table 5
Accuracies of the recognised changed objects on built-up land. The accuracies before recognition are shown in Table 4.

Accuracy	DS1	DS2	DS3	DS4	DS5	DS6
AR	0.893	0.811	0.843	0.977	0.802	0.808
FDR	0.302	0.465	0.449	0.315	0.272	0.334
OA	0.914	0.938	0.954	0.966	0.956	0.899

false alarms. The thresholding parameter T_M for each dataset was set by the trial-and-error strategy, which made the *FDR* decrease the most while kept the *AR* almost the same.

Comparing Tables 4 and 5, we can see that the recognition results have similar *AR*s with those of the changed objects before recognition, but the *FDR*s are 2–4% lower after recognition for DS1, DS4–DS6, and over 10% lower for DS2 and DS3. We can also clearly see the effectiveness of the recognition component in Fig. 9. Generally for all the datasets, many changed objects on non-built-up land were removed after recognition. Specially in DS5 and DS6, some unchanged objects within built-up land were removed by recognition.

4. Discussion

In the proposed framework, change detection was first performed at the pixel level through full use of the spectral and textural information. The changed pixels were then subjected to post-processing operations through mathematical morphology to generate changed objects, which improved both the accuracy and completeness of changed regions, and then achieved the transition from detection at pixel level to the successive analysis at object level. After that, the changed objects were further recognised through the MBI feature to identify changed objects on built-up land from all the generated changed objects. This further improved the accuracy of change detection on built-up land.

In the pixel-level change detection component, the separately adaptive differencing method and logical OR operation was designed to integrate textural and spectral features for completely detecting change. In the experiment, the proposed method was compared with the state-of-the-art pixel- and object-based CVA method based on the same features and post-processing procedures. The better detection capability of the proposed method presented the superiority on detecting changed pixels.

The designed post-processing method optimised the pixel-based change detection and minimised fragmentations of the

changed regions. The shape of the changed region was more complete after post-processing, which facilitated the transition from detection at the pixel level to recognition at the object level. Post-processing using the closing operation and gap filling connected narrow gaps within the changed regions to form closed interconnected regions, which can improve the completeness and detection accuracy of changed regions. Next, the opening operation eliminated the spines on the borders of the regions and broke narrow connections between regions to form unconnected changed regions. The area threshold eliminated insignificant small patches. The above two steps can result in the smoother bounders of detected regions and also lower false alarms. In the post-processing procedures, the window size of the morphological operations was determined by a lot of tests, which were suitable for the experimental images. When the post-processing method is used for other images with higher or lower spatial resolution, the window size should be cautiously set according to testing results. Even though the designed post-processing steps are purely computational operations on image pixels, the improvement of detection capacity is significant as shown in Section 3.3, which justifies the effectiveness of the designed steps. Since the post-processing steps are performed on the detected changed pixels, they would not introduce new fake changed regions. Moreover, the first two steps are the morphological closing and gap filling operations, which can increase the changed pixels, thus, the following morphological opening operation and elimination of small patches would have low risk to eliminate real changes that have been detected by the former detection steps. Because of the effectiveness of the designed post-processing operations, we expect that they have the potential to improve the accuracy and completeness of change detection results of other land cover types for high-spatial resolution images.

The recognition of changed objects on built-up land effectively reduced the false alarms by using the MBI feature to indicate changed buildings. In the experimental results we can see that the recognition can remove many changed objects on non-built-up land and unchanged objects within built-up land. However, from the recognition result in Fig. 9 we can also see that the MBI feature cannot remove some fake changed road objects and it is also not sensitive to the regular farmland objects with spectral changes in DS4. This intrigued us to introduce more object-based recognition method (e.g. Han et al., 2015) into the proposed framework to better understand the change type. Furthermore, from the recognition results of DS6 in Fig. 9, the large difference of sensor angles resulted in many false detections which were not able to be removed by both the post-processing and recognition steps. This could be another working direction to further improve the proposed detection framework.

Generally, the proposed change detection framework includes three components: (i) detection of changed pixels, (ii) generation of changed objects, and (iii) recognition of changed objects on built-up land. The first component tries to detect the change as much as possible and can neglect the problems of the false detections and the completeness of changed regions. Then the second component is to make the change region complete and improve detection accuracy, and then transfer to object-level analysis. The third component cannot gain new change information, but it can further reduce the false detections by object-based recognition. The detection framework is designed for changes of built-up land, where the selected features are closely related to the objects on built-up land. It is noted that the framework has the potential to detect changes of other land cover types by selecting the features relating to the targets. Furthermore, we can also modify the detection methods and selected features in the first and the third components, which could help to expand the framework to object detection applications.

Although the proposed method for change detection of built-up land based on the experimental high-spatial resolution images produced promising detection results, issues involving commission and omission detections still exist because of confounding factors. These include the spectral changes of the same objects, different imaging angles and radiometric conditions during different phases. Even though the spatial resolution of the datasets ranges from 0.5 to 2 m, the detection results of all the datasets are acceptable, which confirms the robustness of the proposed framework to this range of spatial resolution. However, the detection results of GF-1 datasets have larger false alarms than other datasets with higher spatial resolution. This may be caused by the coarse spatial resolution (2 m) of GF-1 images which leads to the higher false alarms at the pixel-level detection steps and less detection capacity improvement at the post-processing steps. Hence, the application potential of the proposed framework to coarser spatial resolution (>2 m) needs to be further verified.

Totally, there were three thresholding parameters needed to be set manually in the proposed framework. We did not focus on automatically setting the parameters but used the trial-and-error strategy in this study. On the other hand, the threshold parameters were global-oriented. We expect that the detection performance can be further improved if the local-oriented thresholding strategy is used in the framework. Hence, how to setting thresholding parameters properly remains a challenge in the future.

5. Conclusion

A framework for change detection of built-up land using a combination of pixel-based change detection and object-based recognition was proposed in the paper. In high-spatial resolution images, built-up land has characteristics of large spectral differences and complex structures. The proposed framework took full advantage of the spectral and textural information contained in the images and was able to determine changes to the geometric properties and attribute values of the built-up land, thus effectively improving the accuracy for monitoring of built-up land change.

Further investigations on the use of textural and shape features are warranted. In addition, the detection process should be improved and made more intelligent through techniques such as machine learning and fuzzy theory. This would minimise the dependence of the change detection process on human–computer interactions.

Acknowledgments

This work was supported by the Visiting Research Scholar Program of the China Scholarship Council (Grant No. 201306195008), the Qinglan Project of Jiangsu Province, China (Grant No. 201423), the Natural Science Foundation of Jiangsu Province, China (Grant No. BK20160623 and BK20131056), and the Natural Science Foundation of Fujian Province, China (Grant No. 2015J01175). The authors acknowledge the National Date Center of High Resolution Earth Observation System for providing the GF-1 images and the Information Center of Land and Resources of Jiangsu Province for providing the aerial photographs. The authors thank Associate Professor Jiangfeng She, Associate Professor Gang Chen, Professor Peijun Du, and Professor Jiechen Wang of the Nanjing University, Chief Engineer Xiaoqun Song of the Information Center of Land and Resources of Jiangsu Province, Director Guofeng Zhou of the Information Center of Land and Resources of Changzhou City, Associate Professor Chenhua Shen of the Nanjing Normal University, and Associate Professor Ke Wang of the Hohai University for their unstinting helps and supports. The authors acknowledge the three anonymous reviewers for their insightful comments and suggestions.

References

Artmann, M., 2014. Assessment of soil sealing management responses, strategies, and targets toward ecologically sustainable urban land use management. Ambio 43 (4), 530–541.

Baatz, M., Schäpe, A., 2000. Multiresolution segmentation—an optimization approach for high quality multi-scale image segmentation. In: Strobl, J., Blaschke, T., Griesebner, G. (Eds.), Angewandte Geographische Informations-Verarbeitung XII. Wichmann Verlag, Karlsruhe, Germany, pp. 12–23.

Ban, Y., Yousif, O.A., 2012. Multitemporal spaceborne SAR data for urban change detection in China. IEEE J. Sel. Top. Appl. 5 (4), 1087–1094.

Blaschke, T., 2010. Object based image analysis for remote sensing. ISPRS J. Photogramm. 65 (1), 2–16.

Blaschke, T., Hay, G.J., Kelly, M., Lang, S., Hofmann, P., Addink, E., Feitosa, R.Q., Meer, F., Werff, H., Coillie, F., Tiede, D., 2014. Geographic object-based image analysis–towards a new paradigm. ISPRS J. Photogramm. 87, 180–191.

Bruzzone, L., Bovolo, F., 2013. A novel framework for the design of change-detection systems for very-high-resolution remote sensing images. Proc. IEEE 101 (3), 609–630.

Bouziani, M., Goïta, K., He, D.C., 2010. Automatic change detection of buildings in urban environment from very high spatial resolution images using existing geodatabase and prior knowledge. ISPRS J. Photogramm. 65 (1), 143–153.

Bovolo, F., Bruzzone, L., 2007. A theoretical framework for unsupervised change detection based on change vector analysis in the polar domain. IEEE Trans. Geosci. Remote 45 (1), 218–236.

Bovolo, F., 2009. A multilevel parcel-based approach to change detection in very high resolution multitemporal images. IEEE Geosci. Remote Sens. Lett. 6 (1), 33–37.

Bovolo, F., Marchesi, S., Bruzzone, L., 2012. A framework for automatic and unsupervised detection of multiple changes in multitemporal images. IEEE Trans. Geosci. Remote 50 (6), 2196–2212.

Carlotto, M.J., 2005. A cluster-based approach for detecting man-made objects and changes in imagery. IEEE Trans. Geosci. Remote 43 (2), 374–387.

Chen, G., Hay, G.J., Carvalho, L.M.T., Wulder, M.A., 2012. Object-based change detection. Int. J. Remote Sens. 33 (14), 4434–4457.

Chen, J., Gong, P., He, C., Pu, R., Shi, P., 2003. Land-use/land-cover change detection using improved change-vector analysis. Photogramm. Eng. Remote Sens. 69 (4), 369–380.

Chen, J., Mao, Z., Philpot, B., Li, J., Pan, D., 2013. Detecting changes in high-resolution satellite coastal imagery using an image object detection approach. Int. J. Remote Sens. 34 (7), 2454–2469.

Clausi, D.A., 2002. An analysis of co-occurrence texture statistics as a function of grey-level quantization. Can. J. Remote Sens. 28 (1), 45–62.

Coppin, P., Jonckheere, I., Nackaerts, K., Muys, B., Lambin, E., 2004. Digital change detection methods in ecosystem monitoring: a review. Int. J. Remote Sens. 25 (9), 1565–1596.

Desclée, B., Bogaert, P., Defourny, P., 2006. Forest change detection by statistical object-based method. Remote Sens. Environ. 102 (1–2), 1–11.

Du, P., Liu, S., Gamba, P., Tan, K., Xia, J., 2012. Fusion of difference images for change detection over urban areas. IEEE J. Sel. Top. Appl. 5 (4), 1076–1086.

Gamba, P., Dell'Acqua, F., Lisini, G., 2006. Change detection of multitemporal SAR data in urban areas combining feature-based and pixel-based techniques. IEEE Trans. Geosci. Remote 44 (10), 2820–2827.

Han, J., Zhang, D., Cheng, G., Guo, L., Ren, J., 2015. Object detection in optical remote sensing images based on weakly supervised learning and high-level feature learning. IEEE Trans. Geosci. Remote 53 (6), 3325–3337.

Haralick, R.M., Shanmugan, K., Dinstein, I., 1973. Textural features for image classification. IEEE Trans. Syst., Man, Cybern. SMC-3 (6), 610–621.

Huang, X., Zhang, L., Zhu, T., 2014. Building change detection from multitemporal high-resolution remotely sensed images based on a morphological building index. IEEE J. Sel. Top. Appl. 7 (1), 105–115.

Hussain, M., Chen, D., Cheng, A., Wei, H., Stanley, D., 2013. Change detection from remotely sensed images: from pixel-based to object-based approaches. ISPRS J. Photogramm. 80, 91–106.

Im, J., Jensen, J.R., Tullis, J.A., 2008. Object-based change detection using correlation image analysis and image segmentation. Int. J. Remote Sens. 29 (2), 399–423.

Johansen, K., Arroyo, L.A., Phinn, S., Witte, C., 2010. Comparison of geo-object based and pixel-based change detection of riparian environments using high spatial resolution multi-spectral imagery. Photogramm. Eng. Remote Sens. 76 (2), 123–136.

Johnson, R.D., Kasischke, E.S., 1998. Change vector analysis: a technique for the multispectral monitoring of land cover and condition. Int. J. Remote Sens. 19 (3), 411–426.

Jung, F., 2004. Detecting building changes from multitemporal aerial stereopairs. ISPRS J. Photogramm. 58 (3–4), 187–201.

Kwarteng, A.Y., Chavez, J.P.S., 1998. Change detection study of Kuwait City and environs using multi-temporal Landsat Thematic Mapper data. Int. J. Remote Sens. 19 (9), 1651–1662.

Liu, S., Bruzzone, L., Bovolo, F., Du, P., 2015. Hierarchical unsupervised change detection in multitemporal hyperspectral images. IEEE Trans. Geosci. Remote 53 (1), 244–260.

Listner, C., Niemeyer, I., 2011. Object-based change detection. Photogramm. Fernerkun. 4, 233–245.

Lu, D., Mausel, P., Brondizio, E., Moran, E., 2004. Change detection techniques. Int. J. Remote Sens. 25 (12), 2365–2401.

Nielsen, E.M., Prince, S.D., Koeln, G.T., 2008. Wetland change mapping for the US Mid-Atlantic region using an outlier detection technique. Remote Sens. Environ. 112 (11), 4061–4074.

Pesaresi, M., Ehrlich, D., Caravaggi, I., Kauffmann, M., Louvrier, C., 2011. Toward global automatic built-up area recognition using optical VHR imagery. IEEE J. Sel. Top. Appl. 4 (4), 923–934.

Prakash, A., Gupta, R.P., 1998. Land-use mapping and change detection in a coal mining area–a case study in the Jharia coalfield, India. Int. J. Remote Sens. 19 (3), 391–410.

Schott, J.R., Salvaggio, C., Volchok, W.J., 1988. Radiometric scene normalization using pseudoinvariant features. Remote Sens. Environ. 26 (1), 1–16.

Singh, A., 1989. Digital change detection techniques using remotely-sensed data. Int. J. Remote Sens. 10 (6), 989–1003.

Sohl, T.L., 1999. Change analysis in the United Arab Emirates: an investigation of techniques. Photogramm. Eng. Remote Sens. 65 (4), 475–484.

Stow, D., Hamada, Y., Coulter, L., Anguelova, Z., 2008. Monitoring shrubland habitat changes through object-based change identification with airborne multispectral imagery. Remote Sens. Environ. 112 (3), 1051–1061.

Volpi, M., Tuia, D., Bovolo, F., Kanevski, M., Bruzzone, L., 2013. Supervised change detection in VHR images using contextual information and support vector machines. Int. J. Appl. Earth Obs. 20, 77–85.

Xiao, P., Wang, X., Feng, X., Zhang, X., Yang, Y., 2014. Detecting China's urban expansion over the past three decades using nighttime light data. IEEE J. Sel. Top. Appl. 7 (10), 4095–4106.

Yousif, O., Ban, Y., 2013. Improving urban change detection from multitemporal SAR images using PCA-NLM. IEEE Trans. Geosci. Remote 51 (4), 2032–2041.

Yuan, F., Sawaya, K.E., Loeffelholz, B.C., Bauer, M.E., 2005. Land cover classification and change analysis of the Twin Cities (Minnesota) Metropolitan Area by multitemporal Landsat remote sensing. Remote Sens. Environ. 98 (2), 317–328.